Tectonic Critical Phenomena with Dilatancy in Lithosphere Sections

Gerd Gudehus [1)] and Christof Lempp [2)]

1) Institute of Soil and Rock Mechanics, Karlsruhe Institute of Technology, Gerd.Gudehus@kit.edu
2) Institute of Geosciences and Geography, Martin-Luther University Halle, christof.lempp@geo.uni-halle.de

Keywords: critical phenomena, fractality, dilatancy, contractancy, shear bands, stress-dilatancy, collapse, chain reactions, seismicity, shear wave splitting, Lévy process

Abstract

Observations in the lithosphere show that driven critical phenomena with dilatancy can lead to spontaneous phenomena with contractancy of the pore system like in lab tests. Their spatial and temporal fractality with variable exponents just below 1 is revealed by borehole loggings and tails of seismic spectra. Evaluations of seismograms, justified by means of a fractional wave equation with stress-dependent incremental stiffness, match nearly equal directions of stress and tectonic stretching rate tensors. Splitting of shear waves confirms that a driven stressing implies dilatancy and that seismogenic chain reactions, enhanced by shock waves and pore pressure increase, imply contractancy and a drop of deviatoric stress. Except rockbursts by excessive pore pressures, this holds true from ca 1 km depth down to the upper mantle in subduction zones. The randomness of such successive critical phenomena is captured by stable Lévy processes, this is confirmed by data plots from a subduction zone and a pumping test in a graben. The employed field theory could be further developed with observations in the lab and in situ.

1 Introduction

Fault patterns in pieces of rock, in outcrops, and in wider regions are often similar (Fig. 1) and indicate geometrical fractality (Mandelbrot 1982). Heidbach et al. (2018) present directions of maximal horizontal stress of tectonically active lithosphere parts. Amounts of stress depend on the size of inspection or calculation grids, but their directional features are scale-independent, which speaks for fractal distributions of geometrical and mechanical quantities. Wildly random (Mandelbrot 1999), spatial fluctuations with divergent wavelengths are frozen relics of critical phenomena (Sornette 2000). Listing main open questions of structural geology and tectonics, Gudmundsson (2013)

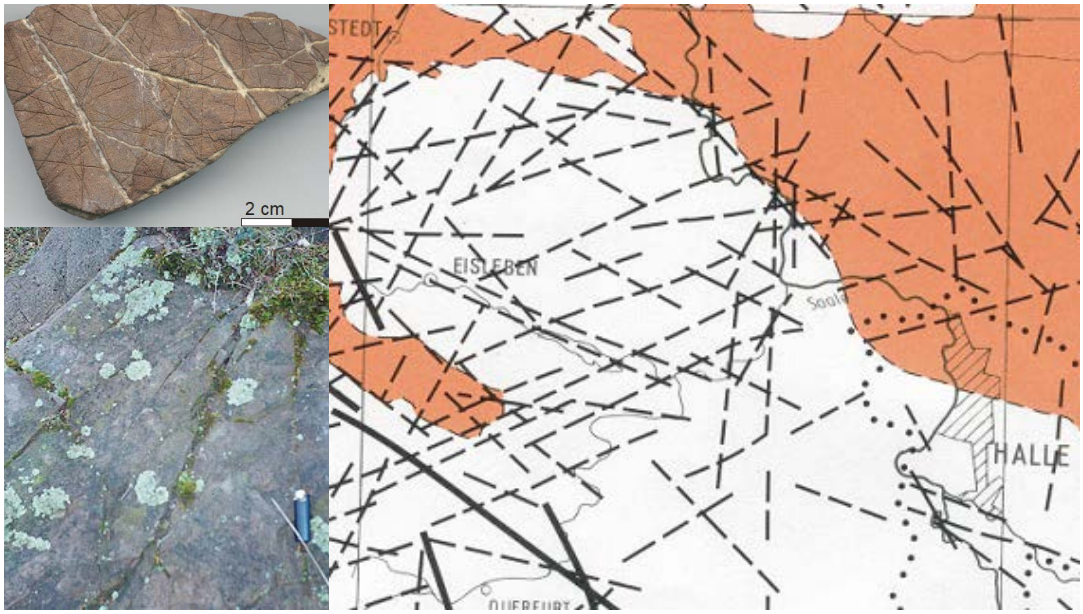

Figure 1: Similar fault patterns in a piece of rock, a horizontal outcrop and a structural-geological map within the North-German Basin (Lempp, for lectures)

points also to Sornette's pioneer book. So how could the variable fractality of faults and cracks in the lithosphere be captured by means of critical phenomena with dilatancy?

The evolution of the lithosphere is driven by the upper mantle, and less also by changes at and near the free surface. These boundary conditions are partly periodic from gravity and partly less regular due to critical phenomena. Lithosphere sections, which may be laterally delimited by main faults, are transported along other with internal forces along suitably chosen lateral and basal boundaries. Stresses, pore pressures and/or deformations are no drive like with samples in a triaxial setup, or nearly so in model tests: lithosphere sections are rather arbitrarily delimited and have no well-defined initial and boundary conditions, and fluctuation wavelengths are not confined as in lab tests. So how far can driven stressing with dilatancy and seismogenic stress-drop with contractancy evolve *in situ* like in the lab?

In the companion paper (Gudehus and Lempp 2022) - abbreviated TDA in the sequel for tectonics, dilatancy and analogue - we present critical phenomena with dilatancy and contractancy in analogue models. In the present paper we show that the same features appear in lithosphere sections, why and how the randomness is wilder (i.e. more markedly stochastically fractal) *in situ* than in the lab, and what could be further done. For this purpose we outline first methods for observing lithosphere sections (Sect. 2), then findings from exemplary regions (Sect. 3). Thereafter the wild randomness of successive driven

dilatation and spontaneous contraction with seismicity is analyzed (Sect. 4).

We conclude that there are scale-independent features which can be captured by means of an extended field theory, and add an outlook (Sect. 5). Mathematical details are outlined in the Appendix, as in TDA this clarification is indispensable despite or just due to the complexity and opacity of the lithosphere.

2 Methods for observing lithosphere sections

Density and stress

We employ *inspection cubes* of suitably chosen width d so that quasi-local quantities are mean values with fractal uniformity (Appendix A2 of TDA), and focus on ranges with dominant shear bands (faults). At a lower bound $d = d_r$ fractal patterns make just sense, and below an upper bound vanishing fractional gradients are equivalent to fractal uniformity. In between masses and energies in a cube are proportional to $(d/d_r)^{3\alpha}$ with α just below 1 ($\alpha = 1$ without fractality), while the coefficient of variation and quasi-local directions are rather d-independent (visible e.g. with Fig. 1). These properties are inevitably idealized, as are constitutive relations with quasi-local and -momentary quantities (TDA, A4), and the range of validity cannot be precisely determined.

Different to the pore water pressure p_w the quasi-local *effective stress tensor* $\hat{\sigma}'_{ij}$ cannot be observed directly, and indirect estimates of the same are imprecise due to fractal and non-fractal inhomogeneities. In the case of a horizontal surface and horizontal fractal uniformity the vertical principal stress $\hat{\sigma}'_1$ can be estimated from overburden and p_w, the direction of $\hat{\sigma}'_2$ is indicated by the ovalization of vertical boreholes, and the smallest principal stress $\hat{\sigma}'_3$ can be estimated by means of hydraulic fracturing. Within a fractally uniform range the mean pressure $\hat{p}' = \frac{1}{3}\hat{\sigma}'_{ii}$ (summation for i) decreases with a growing size d of inspection cubes like the bulk density $\hat{\rho}_s$ by a power-law (TDA, A2 and A4).

Outcrops can exhibit *fractal fault patterns*, but such relics of critical phenomena can but crudely indicate the d-dependence of the density $\hat{\rho}_s$ of the solid fabric. Taking over the distinction from multi-stage triaxial tests (TDA, Sect. 4), dominance of faults requires that the smallest principal effective stress $\hat{\sigma}'_3$ exceeds the effective cohesion $\hat{c}'$ in a quasi-local sense. Combining parameters of sandstone and granite with hydrostatic pore water shows that this holds below about 1 km depth with normal and/or strike-slip faulting (given e.g. for Fig. 4 in Sect. 3). Due to the ever-present fractality borehole ovalizations can but roughly exhibit far-field directions of the horizontal intermediate effective principal stress $\hat{\sigma}'_2$, and hydraulic fracturing can roughly indicate the far-field $\hat{\sigma}'_3$. Cracks arise near deeper boreholes as the difference of supporting suspension pressure and hydrostatic p_w does not reach the far-field $\hat{\sigma}'_3$. Wider deep cracks can arise with

injection or natural excessive pore water pressure p_w, especially by the accumulation of natural gas under caprocks (GUDEHUS et al. 2022). The sometimes resulting cold volcanism implies a localization of fluid flow into channels which eludes our distinction from dominant faults by means of $\hat{\sigma}_3'$ and $\hat{c}'$.

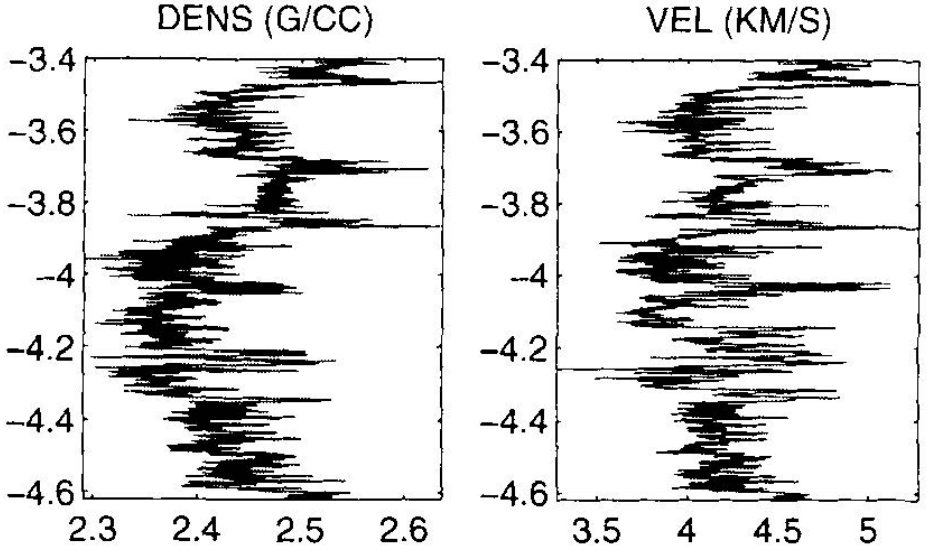

Figure 2: Distributions of density (left) and shear wave speed (right) versus depth in km along an almost horizontal borehole in sandstone under the North Sea (LEARY 1997, part of Fig. 4b). Depths below 3.4 km indicate lengths along the borehole up to about 10 km

Distributions of logging data along boreholes (LEARY 1997) can indicate fractal uniformity, e.g. for an almost horizontal borehole under the North Sea (Fig. 2). The bulk mass density $\rho_s = \gamma_s/g$ of the porous solid fabric and its velocity c_s of shear waves, which are related via the shear modulus G by $c_s = \sqrt{2G/\rho_s}$, fluctuate almost equally along the borehole with wavelengths from about 20 m to 5 km. These bounds are roughly determined by the size of logging devices and by the distance of main faults (GUDEHUS et al. 2022), respectively. The plots indicate a reduction of the quasi-local density $\hat{\rho}_s$ with an increase of the width d of inspection cubes, which can be approximated by $\hat{\rho}_s = (\hat{\rho}_{sr}(d/d_r)^{3(\alpha-1)}$ (TDA, A2) with a fractal exponent α just below 1, while LEARY'S (1997) power spectra are misleading as ρ_s^2 is not proportional to a mechanical power like v^2 from seismograms. A more precise determination of α is impossible even in the case of such a fractal uniformity as borehole data are biased by logging devices.

Seismicity

Apart from volcanism, electromagnetic waves and gravimetry, *seismograms* are the main indicators of in-depth states and changes. As outlined in Appendix A1, the balance of linear momentum for elastic deviations from equilibrium in a fractal solid leads to a fractional wave equation of degree 2α just below 2 both spatially and temporally. Therein the matrix of incremental elastic stiffness is determined by the dependence of the elastic energy on the elastic strain tensor (or equivalently the effective stress tensor) and the pore volume fraction (TDA, A4). With fractal uniformity and α just below 1 plane wave crests propagate with an α-independent speed, and have an increasing attenuation with smaller α due to the fractal diffusion of seismic energy in the elastic range. This theory supports the usual evaluation of seismograms with the wave equation of a non-fractal solid, also with site-dependent wave speeds, but it refutes usual quality-factors for attenuation. However, the fractality of fault patterns prevents precise inversions of seismograms.

Lengths l of *seismic waves* (calculated from frequencies f and wave speeds c by $l = c/f$) can roughly delimit inspection cubes with fractal uniformity, and polarizations of waves can indicate the orientation of the solid fabric and its stress, but not precisely due to fractal fluctuations. Observed tails of power spectra tend to $v^2 \propto f^{-2\alpha}$ with α just below 1, so their lower bounds or corner frequencies indicate upper bounds of fractal uniformity (A2 of TDA). This is justified by a fractional wave equation (A1), but implies an imprecision due to the fractal diffusion of seismic energy. As outlined e.g. by the Committee on Earthquakes (2003), momentum magnitudes M_m are roughly proportional to kinetic magnitudes $M_v \propto \log v_{max}^2$ with the maximal velocity v_{max} of an earthquake for a minimal frequency f_{min}. The implied fractal similarity of differently big earthquakes explains the empirical power-law relation of corner frequencies with sizes of seismogenic zones, and matches α just below 1 from spectral tails of M_m versus f_{min} for ensembles of earthquakes (Denolle and Shearer 2016) instead of $\log v^2$ versus f for a single seismic episode.

Focussing on driven dilatant and spontaneous contractant critical phenomena, we presume critical points and component ratios of quasi-local and quasi-momentary stretching (Appendix A1) with a *maximal rate of dissipation* for a given quasi-local stress tensor (TDA, A4). This universal principle supports an invariant stress-dilatancy relation and the coaxiality of quasi-local and -momentary stress and stretching rate tensors. The ensued diffusion of pore water eludes Darcy's law and the classical balance equation of water mass as the pore system is rather fractal. Thus the enhancement of the tectonic drive by an increase of pore water pressure could be estimated, but the calculation of hydraulic delay times with a fractional diffusion equation (A1) is only a first step.

Fault plane solutions and moment magnitudes presume punctual stress drops (Madariaga 2007), but earthquakes evolve in *mechanical chain reactions*. After a driven stressing with dilatation they begin (nucleate) where the quasi-local specific elastic energy attains a tipping point with regard to the pore volume fraction (TDA, A4). S-waves arise with an alignment according to maximal dissipation as saddle points of the elastic energy entail its steepest descent, and P-waves arise as the sudden contraction of the fabric is impeded by pore water. Seismic waves and pore pressure increases trigger further collapses as far as the neighborhood is equally aligned and almost critical, thus wavelengths are confined. The collapse front widens slower laterally than a P-wave (ca 3 to 5 km/s as against c_p from ca 5 to 10 km/s), and proceeds slower with hydraulic diffusion, viz. from ca 1.5 to 3 km/s (Committee on Earthquakes 2003). Each seismogenic chain reaction leaves back a reduced ratio $\hat{\tau}/\hat{p}'$ of quasi-local invariant shear stress $\hat{\tau}$ and directionally mean effective pressure $\hat{p}'$, and a lower pore volume fraction $\hat{n}$. Thereafter both ratios rise again with a continued tectonic drive, but not at the same site and with the same size as before due to fractal (i.e wild or non-Gaussian) fluctuations. The dwindling quasi-local cohesion $\hat{c}'$ can be partly regained in sufficiently long aseismic intervals by condensation and cold welding.

We agree with Leary's (1997) view that subcritical clusters of different sizes can get critical, but with wild fluctuations and not mild ones as by classical thermodynamics which he employs. Seismogenic chain reactions can attain extremely different sizes, each one requires quasi-locally a uniform stress alignment. They are blocked by a non-critical surroundings wherein further losses of equilibrium cannot be triggered. We reject the 'dilatancy-diffusion hypothesis' beyond the arguments of Bakhmutov and Groza (2008) and of Main et al. (2012): dilatancy means a relation of dilatation by shearing with a growing ratio of shear stress and effective pressure, but a diffusion of pore water - driven by a sudden rise of its pressure, as pointed out by the same authors - occurs only after a collapse with a contraction, not during the previous dilatation as this is too slow for reducing the pore water pressure.

Splitting of shear waves

Crampin and Peacock (2008) argue by means of *shear wave splitting* (SWS) that cracks widen prior to an earthquake and close again with the same. SWS means birefringence in an anisotropic solid: an S-wave entering along a principal axis is split into a likewise aligned S-wave and a faster orthogonally polarized one. The authors propose that the alignment by SWS exhibits the one of principal stresses, and that the delay between faster and slower split S-waves indicates the width of stress-aligned penny-shaped cracks. They show with examples that SWS occurs from depths of about 1 km down to the upper mantle, and conclude that the tectonic build-up of stress in a 'subcritical process' is accompanied by a widening of cracks up to a percolation, while earthquakes imply a further

delay of the slower S-wave with a switch of SWS due to a closure of cracks and a stress-drop of the rock mass, respectively. Their arguments speak for successions of driven dilatant and spontaneous contractant critical phenomena, although fractal patterns of faults - and not of cracks without fractality, opening up to a percolation - dominate in the lithosphere below about 1 km depth as outlined further above.

SWS in a fractal solid results from a fractional eigenvalue problem with a stress-aligned orthogonal elastic anisotropy due to a driven succession of saddle points (Appendix A1). The switch of SWS after a collapse can be attributed to a switch of quasi-local principal stresses $\hat{\sigma}_2'$ and $\hat{\sigma}_3'$ during the co-seismic stress-drop, while the pre-seismic orientation of both is regained with a continued tectonic drive. These arguments show why SWS is observable despite fractal fluctuations: successive driven bifurcations can yield a fractally uniform alignment, and with subcritical states near a collapse contractant chain reactions can be triggered by minor disturbances. SWS was not only observed in oil and gas fields with horizontally neighbored wave sources and wavelengths of roughly 1 km (Crampin and Peacock 2008), but also in subduction zones with up to about 200 km long waves from distant sources via the asthenosphere (Lynner and Long 2014). Experiments with diamond-anvil cells reveal that dilatating shear bands and contractant collapses can occur likewise in the upper mantle (Tomioka and Okruchi 2017, Ishii and Ohtani 2021), which matches these observations. This points to fractal fault patterns in the upper mantle with widths of up to about 200 km.

3 Tectonic examples with dilatancy and contractancy

A basin

Lerche and Lempp (2006) compare stress directions of the *North-German Basin* (NGB) with orientations of faults (Fig. 3). Crystalline formations prevail from about 7 km downwards, overlain by roughly 4 km sandstone and limestone up to almost 1 km Zechstein (salinar) and younger sediments enclosing salt diapirs. Directions of major horizontal stress below Zechstein, inferred from directions of major convergence of boreholes - which implies a certain fractal uniformity and coaxiality of quasi-local stress and stretching rate tensors (Appendix A1 and A4 of TDA) - are roughly NNW-SSE (Fig. 3), while directions above salt are roughly E-W. The difference can be attributed to relaxation and diapirs of the salinar, which means an uncoupling of upper formations from lower ones. Roughly NNW-SSE major fault directions, inferred from outcrops, boreholes and seismic profiles, can be attributed to a long-term WSW-ENE stretching (Gast and Gundlach 2006) and to the repeated Scandinavian glaciation and deglaciation (Uta 2017), both with bending of the continental plate and dilatancy in an upper part.

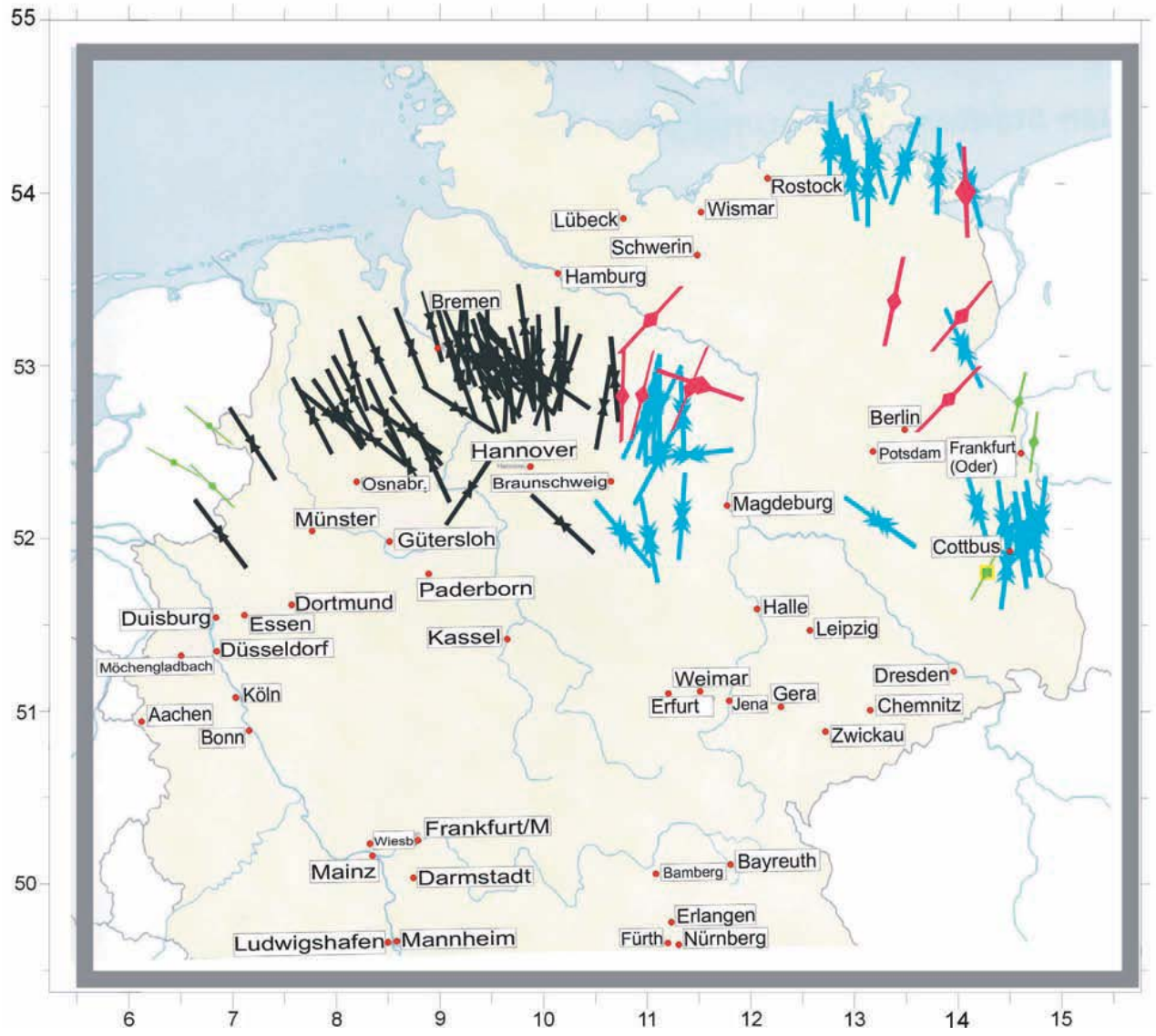

Figure 3: Directions of maximal horizontal stress in the North-German Basin in ca 3 to 7 km depth (Lerche and Lempp 2006). Different arrows indicate different kinds of determination

An evaluation of NGB borehole data (Röckel and Lempp 2003) yields roughly linear increases of quasi-local *stress components* versus depth (Fig. 4). Vertical stresses $\hat{\sigma}_1$ up to 7 km depth were calculated from thickness and density of layers, smallest horizontal stresses $\hat{\sigma}_3$ were determined by hydraulic fracturing, and the pore water pressure (calculated with an elevated specific weight $\gamma_w \approx 11$ kN/m^3 for dissolved salt) was subtracted for getting effective stress components. $\hat{\sigma}'_3$ scatters more than $\hat{\sigma}'_1$ around a linear increase

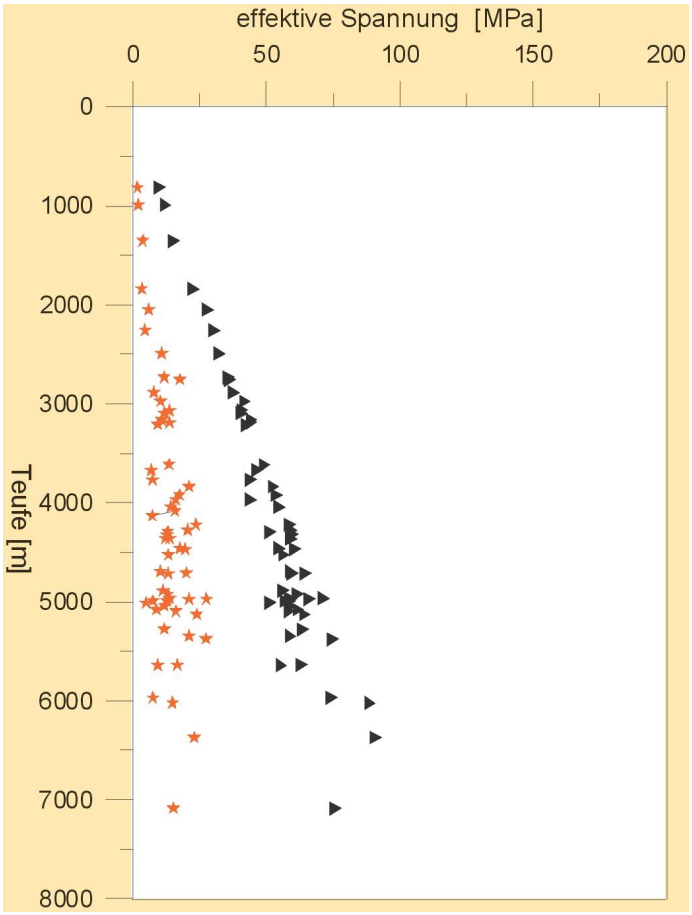

Figure 4: Horizontal (smaller) and vertical (bigger) principal effective stresses versus depth along boreholes in the North-German Basin (Röckel and Lempp 2003)

with depth, and the biggest stress ratios $\hat{\sigma}'_1/\hat{\sigma}'_3$ reach a Mohr-Coulomb limit with $\phi' \approx 40^o$ and $\hat{c}' = 0$. Compared with lab data (Sect. 4 of TDA) this speaks for $\hat{\sigma}'_3 > \hat{c}'$, wherein $\hat{c}'$ is more reduced by dilatation than regained by recrystallization and cold welding, and explains why seismogenic chain reactions are sporadic with the slow tectonic drive.

An evaluation of *satellite data* by Kreemer et al. (2020) leads to wildly scattering horizontal strain rate ellipses for the NGB with an amount of up to 10^{-9} per year, i.e. an overall stretching rate $\hat{D} \approx \frac{1}{3}10^{-16}\mathrm{s}^{-1}$. The employed smoothing-out is questionable for lack of classical differentiability (A1 in the Appendix, and TDA), and the obtained $\hat{D}$ far below the lower bound for inter-crystalline dislocations would exclude tectonic stressing due to thermally activated relaxation (A1 of TDA). However, tectonic dislocations with jerks are much faster than overall reconfigurations (as in lab tests, TDA), while the uncoupling by the salinar further impedes the evaluation of satellite data.

Investigations for *gas fields* in the NGB north of Hannover enable a closer look (Gudehus et al. 2022). A few natural seismic events in the past 20 years had sources in about 20 km to 30 km depth and magnitudes up to 4.3, a medieval one reached about 6. They indicate that tectonic dislocations occurred with jerks above ca 30 km depth (Uta 2017), but not deeper as bending of the continental plate affects mainly the upper crust, while in deeper parts with higher temperatures a deviatoric stress is faster relaxed than built up by the slow tectonic drive. About 20 seismic events were induced by the depletion of gas fields, they had a source depth of ca 5 km and magnitudes up to 3.5. They can be attributed to an additional stretching along the rims of gas fields with an average NNW-SSE alignment, within cubes of about 1 km width, due to the subsidence trough by the depletion. Fault plane solutions indicate an alignment of tectonic dislocations with roughly the same average direction and scattering as in Fig. 3. Power spectra exhibit corner frequencies which indicate wavelengths up to ca 2 km, matching lengths of rim sections of gas fields aligned with main faults.

A graben

Findings in the *Upper Rhine Graben* provide a further confirmation. Fault plane solutions from natural seismicity indicate an E-W overall extension plus an alpine collision, related with normal and strike-slip faulting (Barth et al. 2005). Geodetic measurements indicate overall stretching rates from roughly 10^{-16}/s to 10^{-14}/s with wild spatial and temporal scattering. Seismic sources have depths up to ca 20 km, momentum magnitudes range from ca 2 to 5 within ca 10 years and 300 years, respectively. Barth et al. (2005) conclude that only about 1/10 of the overall relative displacement is co-seismic, and we agree with reservation. Driven tectonic dislocations with minute jerks are not observably seismogenic, while spontaneous ones can be so, but smaller seismic sources are missed by inevitably remote seismometers. The tectonic drive was enhanced in some places by pumping in water for getting geothermal energy (Schoenball 2014): fault plane solutions match the ones of Barth et al. (2005), while lower magnitudes with higher frequencies of episodes were registered in the near-field within a shorter time (Sect. 4).

A subduction zone

The biggest earthquakes occur in *subduction zones*, especially along the coast of Chile (e.g. Fig. 5). Seismic sources accumulate where an oceanic plate hits the continental plate (a), in a deeper shear zone (b), less under the Cordillera (c) and farther offshore (d). The overall tectonic rate of shortening ($\hat{D}$ by A1) is about 500 times the one of the NGB. Sources cannot be allocated to few sporadically active main faults, instead complex fault systems evolve with the incessant drive by the oceanic plate. Sources up to 150 km depth speak for a pre-seismic stressing as the oceanic plate is faster driven downwards than heated and molten, and can arise also below the subducted plate where stressing

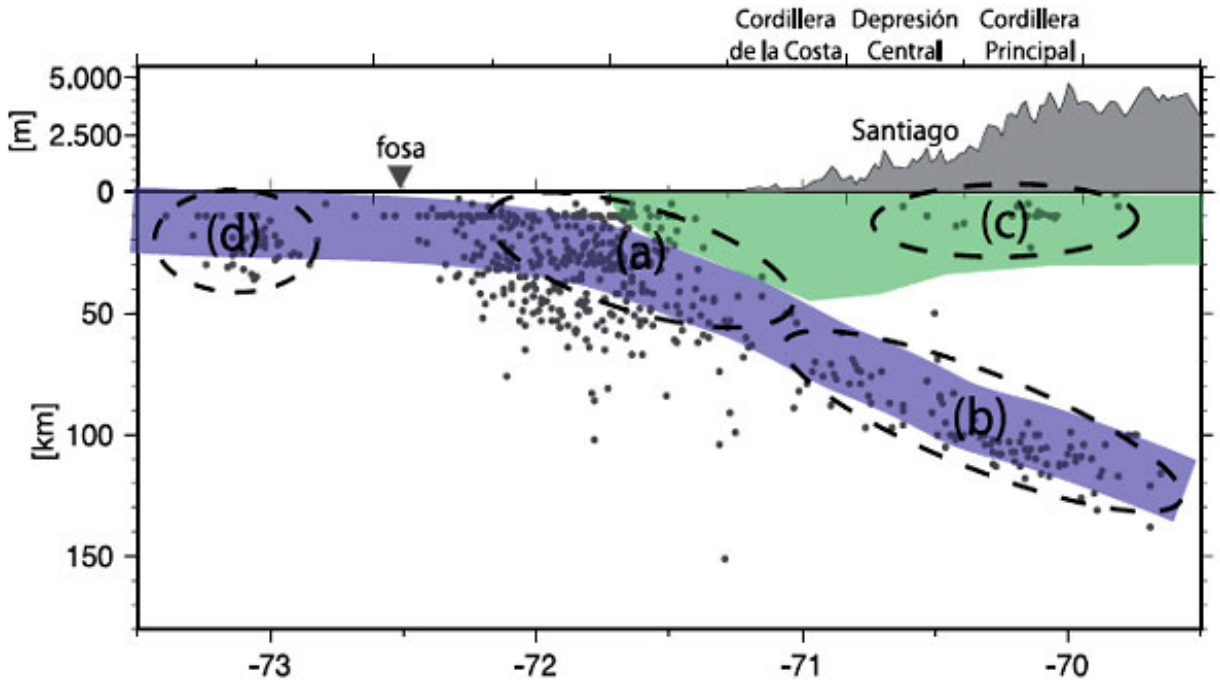

Figure 5: Cross section of central Chile's underground near Santiago with seismic sources (Leighton et al. 2010). Numbers from -70 to -73 denote western latitudes

occurs faster than relaxation. Collapses after driven stressing with a sudden stress-drop occur in a random succession of few big and many small episodes, wherein the smallest ones cannot be discerned due to the depth of sources and the diffusion of seismic energy.

Ground plans with seismic sources under central Chile (Fig. 6) indicate *spatial fractality* for three tectonic settings of Fig. 5. Analyses of the subsequent Maule interplate (thrust) earthquake 2010 with M=8.8 indicate that a collapse front propagated northwards with ca 2 km/s to 2.6 km/s (Sekiguchi et al. 2011). Successive sources of this earthquake have a similar spatial distribution like those in Fig. 6a for many episodes within far longer registration times, alignments by shear wave splitting (SWS) match tectonic ones, source depths range from mainly 10 km to 40 km up to 600 km exceptionally, and SWS delays plus switches indicate a co-seismic contraction alongside with a stress-switch (Torpey 2016). Maximal seismic wavelengths, estimated via corner frequencies (Denolle and Shearer 2016), reach about 200 km, which matches W-E widths of interplate source regions (Fig. 6 a). Gravimetric measurements indicate an overall densification by the same earthquake (Han et al. 2010). Theses findings show both for crust and upper mantle that earthquakes arise after driven dilatation and stressing in mechanical chain reactions with a sudden contraction and stress-switch, and that this occurs repeatedly in a wildly random succession.

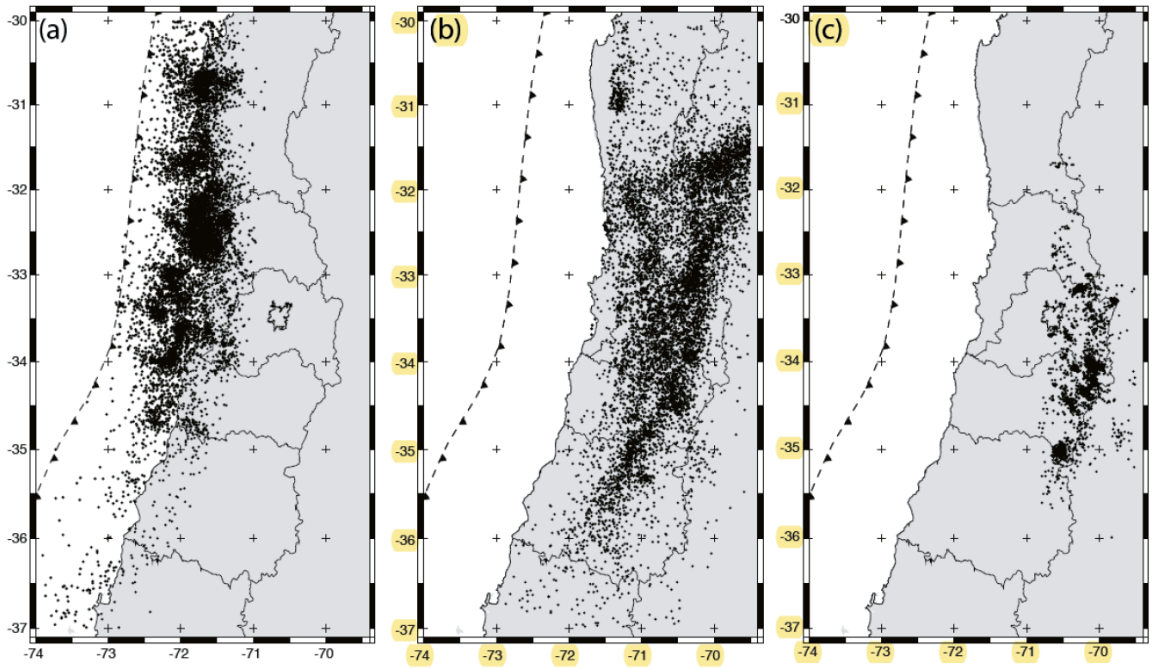

Figure 6: Ground plans with seismic sources of interplate (a), intraplate (b) and crustal (c) earthquakes south of Santiago/Chile (Leighton et al. 2010). Santiago lies about 71 W and 30 S, and the Maule district about 71 W and 35 S

4 Random successions of driven dilatation and spontaneous contraction

Frequency of earthquakes in a subduction zone

Fig. 7 depicts numbers N of earthquakes per year in central Chile, having sources as shown in Fig. 5 and 6, with a magnitude M or more for different source regions and registration times. The regression lines confirm the *Gutenberg-Richter relation* with a negative slope $b \approx 1$. The Gutenberg-Richter magnitude M_v is defined as the logarithm of the energy E radiated from seismic sources by waves within a seismic episode, estimated by means of v_{max} and f_{min} as outlined in Sect. 2, while the moment magnitude M_m refers to the energy dissipated during the sudden stress-drop. Assuming a nearly constant ratio M_v/M_m (Committee on Earthquakes 2003), both magnitudes are equivalent in a plot of $\log N$ versus M except the scaling of E. One can represent each regression line by

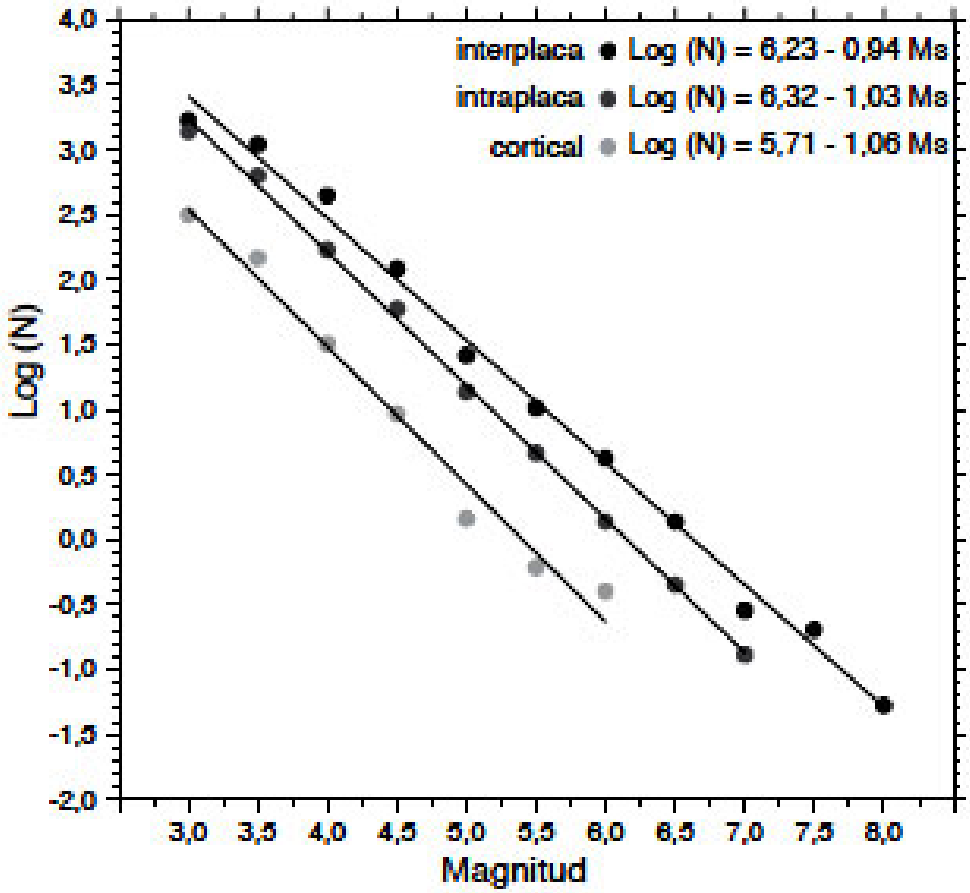

Figure 7: Seismicity of central Chile (Leighton et al. 2010): logarithm of number of earthquakes per year with a given magnitude or greater; upper line interplate (thrust) within ca 300 years, middle line intraplate (subductive shear) within ca 30 years, lower line crustal (under mountains) within ca 3 years

$$N = N_r(E/E_r)^{-b} \text{ for } E_r \leq E \leq E_m \tag{1}$$

with a reference number N_r and an exponent b near 1. The lower cutoff E_r, which serves also as a reference in (1), can be attributed to the confined resolution, while the upper cutoff E_m depends on the tectonic setting and the registration time.

Plots like Fig. 7 can be attributed to *random successions* of driven and spontaneous critical phenomena. The continued tectonic drive stresses and dilatates fractally distributed parts of the lithosphere up to tipping points at thresholds of the elastic energy so that they collapse in mechanical chain reactions, which are enhanced by seismic waves and

pore pressure increases as far as the surroundings is almost critical and the alignment is rather uniform. This happens again in other parts with other sizes and locations (indicated as dots for classically calculated punctual sources in Fig. 5 and 6) by repeated stressing and dilatation after a seismogenic collapse with contraction and stress-drop, and so on in a random succession. The stochastic fractality - or wild randomness in MANDELBROT'S (1999) wording - can be represented by the power-law distribution (1).

Probabilities of seismic episodes

The Chile data set enables a transition to *probabilities* in an inductive way, and in a deductive way which yields more insight. Both approaches require that seismic events can be quantified (which is no more possible with indiscernible small events), counted and added up energetically. Normalizing N by N_r and simplifying with $E_m \gg E_r$, (1) leads to the cumulative probability

$$P = (E/E_r)^{-b} \text{ for } E_r \leq E \leq E_m,\ P = 1 \text{ for } E < E_r,\ P = 0 \text{ for } E > E_m \qquad (2)$$

that an earthquake releases at least the energy E if it occurs in one year in a tectonically defined region for which E ranges from E_r to E_m. Instead, wildly random successions can be considered as *stable Lévy-processes* (Appendix A2). Leaving aside strict definitions and proofs as respective papers and textbooks are hardly readible for non-mathematicians, we focus on the physical meaning of mathematical assumptions. Seismic episodes may be considered as jumps because their duration is far below the one of previous driven stressing with dilatation. Random successions are stochastically stationary as long as stress and pore volume fraction do not change in a long-term average within a lithosphere section. The probability density of events with size E at a time t does not depend on previous ones as with wild fluctuations there is no correlation between subsequent episodes. Lévy-stability means that superpositions lead to a cumulative probability distribution which tends to a power-law with the same exponent.

The energy E of an episode and the registration time t are replaced by $\eta \equiv E/E_r$ and $\tau \equiv t/t_r$ with reference values E_r and t_r, and we confine ourselves to a Lévy-exponent $\gamma = 1$ which implies time-stretching invariance as explained further below. The resulting log-log plot (Fig. 8) exhibits a plateau due to $P \to 1$ for $\eta/\tau \to 0$, a bend at $\eta/\tau = 1$, and a straight line with inclination -1 as asymptote for $\eta/\tau > 1$. This enables an *objective scaling*: the reference energy E_r can be determined - at least principally - by means of the bend of observed $\log N$ plotted versus M, which corresponds to the bend of $\log P$ vs. $\log\eta$ for a given τ. The average recurrence time t_r of events with $E = E_r$ serves as a reference time. This scaling is imprecise due to the entanglement of slow driven and fast spontaneous critical phenomena so that small episodes cannot be precisely discerned.

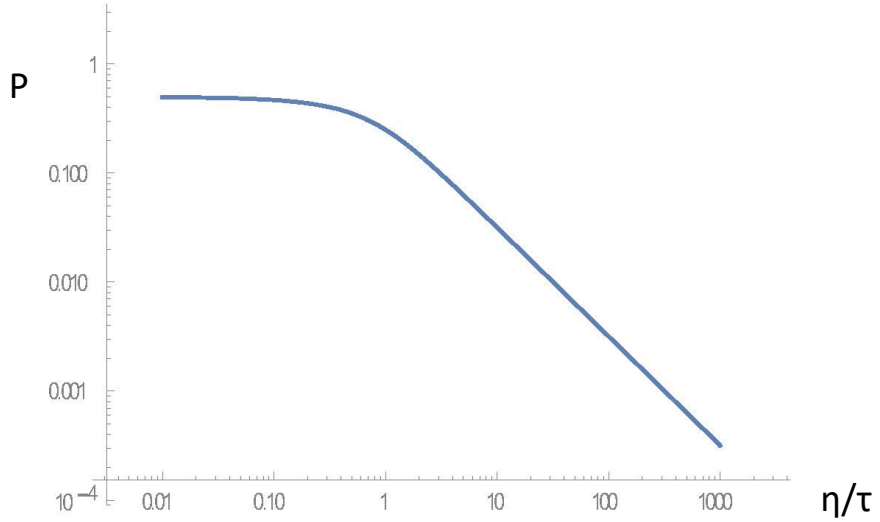

Figure 8: Log-log plot of a stable Lévy distribution with $\gamma = 1$. Cumulative probability P versus η/τ with $\eta \equiv E/E_r$ and $\tau \equiv t/t_r$, cutoffs against $\eta/\tau \to 0$ and $\eta/\tau \to \infty$

Replacing t by the far-field displacement $d = v_p t$ with the average relative far-field velocity v_p of mutually moving plates, one can substitute (2) with $b = 1$ by

$$P \approx \frac{d}{d_r}(E/E_r)^{-1} \text{ for } d/d_r \geq E/E;\ P \approx 1 \text{ for } d/d_r < E/E_r,\ P = 0 \text{ for } E > E_m. \quad (3)$$

This expression differs from (2) by the factor d/d_r and by an objective lower cutoff E_r, while the dependence on E/E_r is the same. While (2) denotes the probability of events per year with E or more if they occur in the range $E_r \leq E \leq E_m$, (3) denotes the probability of such events within a time $t = d/v_p$ for $E \leq E_m$.

The agreement of the $P(E)$-dependence of derived and inferred probabilities, i.e. of (3) and (2) for $b = 1$, results from the *time-stretching invariance* of the lithosphere's response to the tectonic drive. This means that if the far-field driving velocity v_p would be reduced by a factor λ with $0 < \lambda < 1$ the ratio $t/t_r = d/d_r$ would not be changed. In other words, only overall relative displacements of stressing intervals matter for successions of driven and spontaneous critical phenomena (like with sand and rock samples, TDA). Except thermally activated dislocations with soft minerals and/or high temperatures, deviations from $b = 1$ in (1) can be attributed to under- or overestimates of numbers of events with energy E or more due to an insufficient resolution, especially with small magnitudes.

Further validations and limitations

While an objective lower cutoff E_r could be obtained by means of a scaling of E and t via a bent in plots of N versus E, an *upper cutoff* E_m is needed for getting finite mean values and variations. With time-stretching invariance the recurrence time related with E_m would be $t_r E_m/E_r$. As indicated under Fig. 7 the upper cutoff grows in fact with the registration time t, or with the related tectonic displacement $d = v_p t$. This growth could be captured with $E_m = E_{mr} d/d_r$, wherein E_{mr} denotes the upper cutoff for $d = d_r$. A time-independent upper cutoff is given by the size of the seismogenic system, but this is fractally distributed (Leary 1997). Observations of extreme events are too rare for a statistical estimate, so geological considerations and historical reports are indispensable.

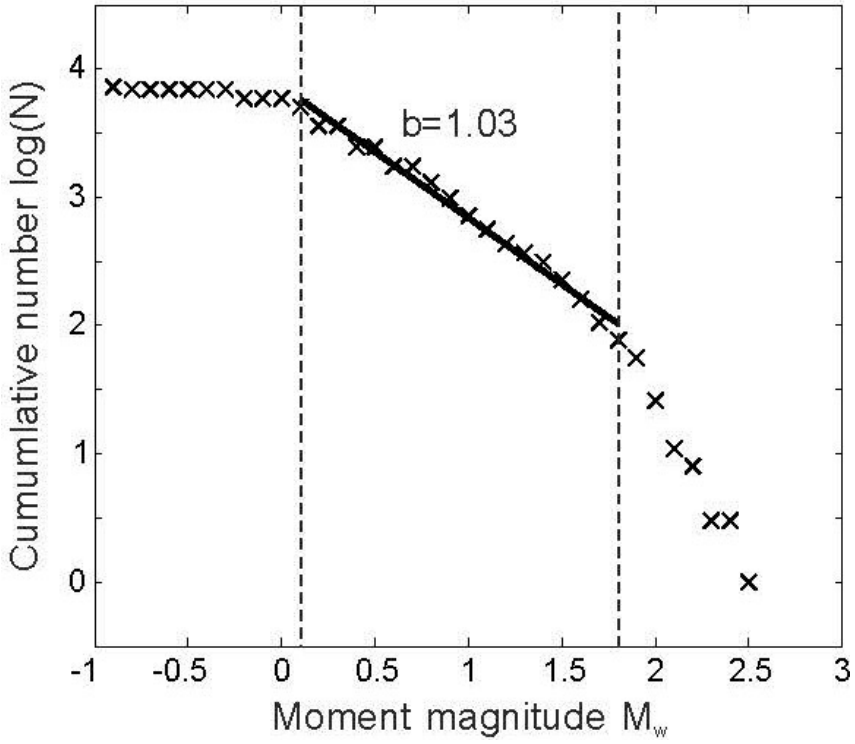

Figure 9: Gutenberg-Richter plot from a pumping test in the Upper Rhine Graben with injection of water in ca 4.5 km depth, with pressures up to ca 13 MPa within ca 12 months, registered with nearby seismometers in ca 2 km to 3 km depth (Schoenball 2014)

The lower cutoff in Fig. 7 is not apt for an objective scaling as it results from the confined resolution. The situation is more favorable e.g. in the Upper Rhine Graben (URG) with a hydraulically induced seismicity. Schoenball (2014) presents a Gutenberg-Richter plot from a field test which shows a plateau, a straight part with $b \approx 1$ and a smooth

upper bound (Fig. 9). The natural tectonic drive by normal and strike-slip faulting is confirmed by satellite monitoring and fault plane solutions (Barth et al. 2005). Despite induced changes of state the enhancement by pumping in water (A1) leads to a stable Lévy-process as cumulative changes of state are minor. The lower bound of the power-law distribution was identified by means of seismometers in nearby boreholes, the upper bound can be attributed to the maximal extent of fracking by injection.

The report by Barth et al. (2005) and an overview for several regions by Godano et al. (2014) are seemingly a counter-evidence as they exhibit scattering b-values below 1 (except the northern URG with $b \approx 1$). Both papers do not indicate bends of log N vs. M despite a systematic influence of registration times. However, regions in the overview were selected by geographic and not by tectonic criteria, and smaller episodes were partly missed due to the confined resolution so that b-values were underestimated. Smooth upper bounds like in Fig. 9 were not attained with natural earthquakes within attainable registration times because of the slow tectonic drive.

(3) enables an estimation of expected values, e.g. of the energy E and of the damage if this is proportional to E (i.e. of the risk), for a relative displacement or an equivalent time, while the coefficient of variation is size-independent due to the fractality. These estimates may be considered as representative for a tectonic region. Quasi-local and -momentary quantities for inspection cubes (as proposed in Sect. 2) are at best simplified expected values. The required random sets could be constructed by means of an extended field theory (A1), but its statistical justification is out of reach. A 'stress-forecast' could principally be achieved with the aid of shear wave splitting (Crampin and Peacock 2008), though with reservation as the relation of stress changes with earthquakes is not unique.

5 Conclusions and outlook

We conclude that tectonic critical phenomena with dilatancy have common features in lithosphere sections and in analogue models, but there are also differences. In both cases patterns of shear bands are rather fractal, indicating a bigger ratio of pore volume for bigger inspection cubes, and there are non-fractal trends due to boundary conditions, which are less known for the lithosphere than in the lab. The dilatancy, i.e. the overall dilatation by shearing with nearly constant pressure, evolves with an increasing ratio $\hat{\tau}/\hat{p}'$ of deviatoric and isotropic quasi-local stress invariants and a decreasing fractal exponent α just below 1, while its negative counterpart or contractancy evolves with a decreasing $\hat{\tau}/\hat{p}'$ and an increasing α. Both in analogue models and in lithosphere sections spatial and temporal distributions are not differentiable so that continuum models do not suffice, and thermodynamic approaches only cannot capture dilatancy and contractancy.

Despite the complexity and opacity of the lithosphere several features are clearly scale-independent. The fractality of fault patterns, exhibited by outcrops and borehole loggings, resembles the one of shear bands at the surface of samples after triaxial tests, but in both cases the fractal exponent α, defined by the power-law dependence of the bulk density on the size of inspection cubes, can only be estimated in a range just below 1. The stress tensor of the rock fabric is not Cauchy's as his volume elements are impossible with shear bands (faults), but due to its symmetry this quasi-local quantity has likewise principal components and directions. Because of fractal fluctuations the latter can at best be estimated by ovalizations of boreholes and hydraulic fracturing.

While geodetic data can at best reveal relative motions of lithosphere sections, seismograms enable a look into the interior despite its fractality. The latter is exhibited by tails of power spectra, which match α just below 1 and indicate upper bounds of fractal uniformity via corner frequencies. The splitting of shear waves (SWS) match the finding with triaxial tests that a driven dilatation can turn into a spontaneous contraction. This holds true down to the upper mantle, which matches findings with diamond-anvil tests while deep fault patterns are indicated indirectly by seismograms. Seismogenic mechanical chain reactions, enhanced by seismic waves and rise of pore water pressures, are testified for minor and strong earthquakes, while their confinement by the one of previously dilatated zones is less regular than with samples in triaxial devices. They can occur down to the asthenosphere under subduction zones, while seismogenic chain reactions with contraction and stress-drop are shallower and rarer in basins and grabens as the overall stretching rate is far lower so that tectonic stressing is slower than thermally activated relaxation below ca 30 km depth.

The relation of stressing and dilatancy can be captured with quasi-local and -momentary quantities by means of a Mohr-Coulomb condition with growing friction and waning cohesion, though less observably *in situ* than in the lab. This holds true as long as the smallest principal stress exceeds the cohesion, which prevails deeper than about 1 km except rockburst due to excessive pore pressures. The implied principle of maximal dissipation justifies the estimate of horizontal directions of principal stresses from the ovalization of boreholes. The contractant collapse with a sudden relaxation beyond a tipping point of the elastic energy with regard to the pore volume is confirmed by a switch of SWS and by a temporary rise of pore water pressure. The probability of seismic episodes due to successions of driven dilatation and spontaneous contraction can be captured as a stable Lévy process, this is validated especially by data from a subduction zone and from a pumping test in a graben.

The proposed concept could be deepened. Scale-independent features could be further clarified by means of sophisticated lab tests and field observations. The employed extended field theory with fractional derivatives, which supports the evaluation of seismograms

and enables energy-based constitutive relations with quasi-local and -momentary quantities, could be worked out more in detail for simulating tectonic successions of critical points with fractional evolution equations. However, the probabilistic interpretation by means of a configurational entropy (TDA) and further tectonic critical phenomena constitute greater challenges.

APPENDIX

A1 Dynamics of lithosphere sections

The balance of linear momentum for a uniformly fractal solid in its elastic range can be captured by the iso-fractional wave equation (Gudehus and Touplikiotis 2016)

$$\hat{\rho}\frac{\partial^{2\alpha}u_i}{\partial t^{2\alpha}} = \hat{M}_{ijkl}\frac{\partial^{2\alpha}u_j}{\partial x_k^\alpha \partial x_l^\alpha}. \tag{4}$$

Therein u_i denotes displacement, $\hat{M}_{ijkl}$ differential stiffness (Appendix A4 of TDA), and $\hat{\rho}$ mass density. t and x_i are normalized by t_r and x_r, respectively (A2 of TDA). Combined with a plane Dirac pulse, Laplace and Fourier transformations of (4) lead to an eigenvalue problem. After diagonalization with the symmetry of $\hat{M}_{ijkl}$, and stretching x_i so that $\hat{M}_{ijkl}$ gets isotropic, reverse transformations lead to a single pulse as fundamental solution (Green's function). Its peak propagates with an α-independent speed for α just below 1, and exhibits a stronger attenuation for lower α. Without stretching of x_i the eigenvalue problem with an anisotropic $\hat{M}_{ijkl}$ (due to anisotropic $\hat{\epsilon}^e_{ij}$ and $\hat{\sigma}'_{ij}$) leads to splitting of a plane shear wave (SWS) propagating along one principal axis if the two other principal components are not equal. Therein the fractional exponent α drops out due to $\alpha = \beta$ (A2 of TDA), thus SWS does not depend on fractality for α just below 1, but requires wavelengths like widths of fractally uniform sections which vary extremely in random successions (A2 in the sequel).

The interaction of solid fabric and pore water with fractality can be captured by the fractional diffusion equation

$$\frac{\partial^\alpha p_w}{\partial t^\alpha} = \frac{\hat{k}_f \hat{K}}{\gamma_w}\frac{\partial^{2\alpha}p_w}{\partial x_i^\alpha \partial x_i^\alpha}, \tag{5}$$

if it occurs in the elastic range and the total pressure $\hat{p}$ is constant. t and x_i must be normalized as for (4), but the reference velocity $v_r = d_r/t_r$ is not the same. With $\alpha = 1$ (5) reduces to a classical diffusion equation, this leads to the estimate for the duration of

hydraulic diffusion given in TDA. (5) is derived from the relation $\hat{v}_{wi} - \hat{v}_{si} = \hat{k}_f \partial^\alpha (\hat{p}_w/\gamma_w + x_3)/\partial x_i^\alpha$ of seepage velocity and hydraulic gradient, and the mass balance $\partial^{2\alpha}(\hat{v}_{wi} - \hat{v}_{si})/\partial x_i^\alpha \partial x_i^\alpha = (\hat{p} - \hat{p}_w)/\hat{K}$ of pore water with the incremental volumetric stiffness $\hat{K}$. Gorenflo and Mainardi (2012) present fundamental solutions of equations like (5), but not with such degrees of fractionality and only with one x.

The multi-fractality, i.e. the spatio-temporal variability of the exponent $\alpha = \beta$ in our case, can be captured by means of variable order fractional operators, especially for diffusion and relaxation beyond classical theories (Chechin et al. 2005). This works for our narrow range of α just below 1 and justifies the use of classical wave and diffusion equations for a first approximation. The practical success matches also the use of stable Lévy distributions.

Outside the elastic range the conservation of masses, energies and momentum could be expressed again by fractional balance equations, wherein the interaction of fabric and pore water is determined by $\hat{\sigma}_{ij} = \hat{\sigma}'_{ij} + \hat{p}_w \delta_{ij}$. However, with the implied non-linear constitutive relations the balance equations are more intricate, so we confine ourselves to qualitative statements for succcessive critical phenomena.

Like with triaxial tests (TDA, A4) an invariant stress-dilatancy relation for driven saddle points of $\hat{w}_e$ implies maximal dissipation, and with it $\hat{\sigma}'_{ij}$ and $\hat{D}^i_{ij}$ are coaxial: -$\hat{\sigma}'_{ij}\hat{D}^i_{ij}$ equals -$\hat{\sigma}'_i\hat{D}^i_i$ with principal components, and is smaller for any deviation of the principal axes of $\hat{D}^i_{ij}$ from the ones of $\hat{\sigma}'_{ij}$ with unchanged $\hat{D}$. A collapse starts again at a tipping point of $\hat{w}_e$ with regard to $\hat{n}$, and the implied contraction with a reduction of the invariant stress ratio $\hat{\tau}/\hat{p}'$ is also captured by the constitutive relation proposed in Appendix A4 of TDA.

Tectonic drives are enhanced by an increase $\Delta\hat{p}_w$ of pore water pressure. As long as with it $\hat{p}$ and $\hat{\tau}$ are not changed $\hat{\tau}/\hat{p}'^f$ increases to $\hat{\tau}/(\hat{p}'^f - \Delta p_w)$. With full saturation a quasi-local $\Delta\hat{p}_w$ would be determined by the incompressibility of mineral and water (like with rock samples, TDA), but the subsequent diffusion of pore water could but crudely be estimated by (5) as the synchronous contraction is not only elastic. Numerical simulations, with the constitutive relations proposed in A4 of TDA and fractional balance equations, could start with the classical $\alpha = 1$ and could proceed with homotopy for lower α. They require initial and boundary conditions which are not precisely known as successions of slow tectonic drive and seismogenic collapse are wildly random.

A2 Lévy distributions

A random succession of seismic episodes with released energy E in the course of a time t is idealized as a stochastic process with E-jumps (e.g. Bertoin 1998). The probability

distribution is assumed to be stable, i.e. to remain the same for superpositions of random quantities. For invariance with regard to units of energy and time we use $\eta \equiv E/E_r$ and $\tau \equiv t/t_r$ by means of reference quantities E_r and t_r. A stable Lévy process is described by a probability density distribution $p(\eta, \tau) \equiv -\partial P/\partial\eta$ with five mathematical assumptions. The first one, viz. $P = 0$ for $\tau = 0$, is evident: the cumulative probability of a seismic event at the onset of registration is zero. The second one, viz. continuity of $p(\eta, \tau)$ versus τ, is legitimate as the tectonic drive is continuous. The third one, viz. that $p(\eta-\eta_s, \tau-s)$ for intervals with $\tau > s$ and $\eta_s = \eta(\tau_s)$ does not depend on the onset s, means stochastic stationarity. The fourth one, viz. that $p(\eta, \tau)$ does not depend on any previous p, is legitimate as any subsequent chain reaction arises in another subregion so that it is not correlated with previous episodes.

The probability density p derived from these assumptions can be represented as the Fourier inversion of the exponential of a sum of three η-dependent terms multiplied with τ. One of them depicts a Gaussian fluctuation, which is not applicable as successions of E-jumps are not mildly random. The second term vanishes as $p(\eta, \tau)$ is one-sided due to $\eta \geq 0$. The third term, written as an integral in general, represents jumps. Its simplest version captures successions of jumps, for the cumulative probability of which

$$P(\eta, a\tau) = P(a^{1/\gamma}\eta, \tau) \tag{6}$$

holds with any $a > 0$, $\eta \geq 0$ and $0 < \gamma < 2$ (Gorenflo and Mainardi 2012). Then $P(\eta, \tau)$ reduces to $P(\eta/\tau^\gamma)$, and the approximation

$$P(\eta, \tau) \approx \tau/\eta^\gamma \text{ for } \eta/\tau^\gamma \geq 1;\ P \approx 1 \text{ for } \eta/\tau^\gamma < 1 \tag{7}$$

holds with an underestimation of P near $\tau/\eta^\gamma = 1$. We focus on γ=1, which means that $P(\eta/\tau^\gamma)$ is not changed if η and τ are stretched by the same factor. For this case the cumulative stable Lévy distribution reads

$$P(\eta, \tau) = 1 - \frac{2}{\pi}\arctan(\eta/\tau). \tag{8}$$

.

Its log-log plot (Fig. 8) exhibits a plateau due to $P \to 1$ for $\eta/\tau \to 0$, a bend at $\eta/\tau = 1$, and a straight line with inclination -1 as asymptote for $\eta/\tau > 1$. In the approximation by (7) with $\gamma = 1$ a sharp bend replaces the mild one by (8).

Expected value and variance of η by (8) with a fixed τ diverge, this is avoided with an upper cutoff. A smooth cutoff instead of an abrupt one (visible e.g. in Fig. 9) widens the range of stability (Schinckus 2013), while a summation of random variables with a truncated stable Lévy distribution converges to a normal distribution only for an extremely big number of summands (Mantegna and Stanley 1994).

The scaling by means of the bend of observed $\log N$ plotted versus $\log E$ is imprecise due to the entanglement of slow driven and fast spontaneous critical phenomena so that episodes cannot be strictly discerned, but it is objective if E_r and t_r are estimated by means of field data. Then the approximation (7) for $\gamma = 1$ can be written

$$P(E,t) \approx \frac{t/t_r}{E/E_r} \text{ for } t/t_r \geq E/E_r;\ P \approx 1 \text{ for } t/t_r < E/E_r. \tag{9}$$

The recurrence time t_r of an event with $E = E_r$ can be replaced by the displacement $d_r = v_p t_r$ with the velocity v_p of tectonic plates past each other in the far-field. Thus (9) can be replaced by (3) due to the stretching-invariance with $\gamma = 1$.

References

Bakhmutov V.G. and Groza A.A. (2008): The dilatancy-diffusion model: new prospects. *Proc. 7th Int. Conf. "Problems of Geocosmos"*, St. Petersburg, Russia, 26-30 May.

Barth A., Ritter J.R.R. and Wenzel F. (2005): Spatial variations of earthquake occurrence and coseismic deformation in the Upper Rhine Graben, Central Europe. *Tectonophysics* 651–652, 172–185.

Bertoin J. (1998): *Lévy Processes*. 278 p., Cambridge Univ. Press, Paperback edition.

Chechkin A.V., Gorenflo R. and Sokolov I.M. (2005): Fractional diffusion in inhomogeneous media. *J. Phys. A: Math. Gen.*, 38, 679–L684.

Committee on Earthquakes (2003): Earthquake Physics and Fault-System Science. *US Nat. Ac. Press*.

Crampin S. and Peacock S. (2008): A review of the current understanding of the seismic shear wave splitting in the Earth's crust and common fallacies in understanding. *Science Direct, Wave Motion* 45, 675-722.

Denolle M.A. and Shearer P.M. (2016): New perspectives on self-similarity for shallow thrust earthquakes. *J. Geoph. Res, Solid Earth*, 121/9, 6533-6565.

Gast R. and Gundlach T. (2006): Permian strike-slip and extensional tectonics in Lower Saxony, Germany. *Zeitschr. Dtsch. Ges. Geowiss.*, 157/1, 41-56.

Godano C., Lippiello E. and de Arcangelis L. (2014): Variability of the b value in the Gutenberg–Richter distribution. *Geophys. J. Int.*, GJI Seismology, 199, 1765–1771.

Gorenflo R. and Mainardi F. (2012): Parametric subordination in fractional diffusion processes. *Fractional Dynamics, Recent Advances*, World Scientific, Singapore, 227-261, arXiv:1210.8414 [math.PR].

Gudehus G. and Lempp, C. (2022): Tectonic Critical Phenomena with Dilatancy in Analogue Models. *Hall. Jb. Geowissenschaftren.*, 45, 1-31.

Gudehus G. and Touplikiotis A. (2016): Wave propagation with energy diffusion in a fractal solid and its fractional image. *Soil Dyn. Earthquake Engng.*, 89, 38-48.

Gudehus G., Lempp C., Müller B., Scheffzük C. and Schilling F. (2022): Depletion-induced seismicity: lessons from comprehensive investigations. *Acta Geotechnica*. https://link.springer.com/article/10.1007/s11440-022-01513-9

Gudmundsson A. (2013): Great challenges in structural geology and tectonics. *Frontiers in Earth Sciences*, Specialty Grand Challenge Article.

Han S.-C., Sauber J. and Luthke S. (2010): Regional gravity decrease after the 2010 Maule (Chile) earthquake indicates large-scale mass redistribution. *Geoph. Res. Lett.*, 37, L23307. https://doi.org/10.1029/2010GL045449

Heidbach O., Rajabi M., Cui X., Fuchs K., Müeller B., Reinecker J., Reiter K., Tingay M., Wenzel F., Xie F., Ziegler M.O., Zoback M.-L. and Zoback M.D. (2018): The World Stress Map database release 2016: Crustal stress pattern across scales. *Tectonophysics*, 744, 484-498.

Ishii T. and Ohtani E. (2021): Dry metastable olivine and slab deformation in a wet subducting slab. *Nature Geoscience*, 14/7, 1-5. DOI:10.1038/s41561-021-00756-7

Kreemer C., Blewitt G. and Davis P.M. (2020): Geodetic evidence for a buoyant mantle plume beneath the Eifel volcanic area, NW Europe. *Geophys. J. Int.*, GJI Geodynamics and tectonics, 222/2, 1316-1332. https://doi.org/10.1093/gji/ggaa227

Leary P.C. (1997): Rock as a critical-point system and the inherent implausibility of reliable earthquake prediction. *Geoph. J. Int.*, 131,451-466. https://doi.org/10.1111/j.1365-246X.1997.tb06589.x

Leighton F., Ruiz S. and Sepulveda S.A. (2010): Reevaluacion del peligro sismico probabilistico en Chile central. *Andean Geology*, 37/2, 455-472.

Lerche I. and Lempp C. (2006): Correlation of stress directions across the North German Basin: suprasalt and subsalt differences. *Ztschr. Dtsch. Ges. Geowiss.*, 157/2, 279–298.

Lynner C. and Long M.D. (2014): Sub-slab anisotropy beneath the Sumatra and circum-Pacific subduction zones from source-side shear wave splitting observations. *Geochem., Geophys., Geosyst.*, 15, 2262-2281. https://doi.org/10.1002/2014GC005239

Main I.G., Bell A.F., Mereduth P. and Touati S. (2012): The dilatancy-diffusion hypothesis and earthquake predictability. *Geol. Soc. London*, Special Publ. 367/1, 215-230.

Madariaga R. (2007): *Seismic Source Theory.* In: Schubert, G. (ed.): Earthquake Seismology. Treatise on Geophysics, 4, 59,82. Elsevier. DOI:10.1016/B978-0-444-53802-4.00070-1

Mandelbrot B. (1982): *The fractal Geometry of Nature.* 460 p., Freeman.

Mandelbrot B. (1999): *Multifractals and 1/f-noise - wild self-affinity in physics.* 450 p., Springer.

Mantegna R. N. and Stanley H. E. (1994): Stochastic Process with Ultraslow Convergence to a Gaussian: The Truncated Lévy Flight. *Physical Review Letters*, Vol. 73/22, 2946-2949.

Röckel T. and Lempp C. (2003): Der Spannungszustand im Norddeutschen Becken. *Erdöl Erdgas Kohle*, 119/2, 73-80.

Schinckus C. (2013): How Physicists Made Stable Lévy Processes Physically Plausible. *Braz. Journ. Phys.*, 43, 281-293.

Schoenball M. (2014): Evolution of stress and seismicity in fractured geothermal reservoirs. *Dissertation Karlsruher Inst. Technol.*, 125 p. DOI: 10.5445/IR/1000041150

Sekiguchi T., Pulido N., Shoji G., Alba J. and Lazares F. (2011): Strong Ground Motions and Site Effects of the 2010 Chile Earthquake. *8th Int, Conf. Urb. Earthq. Engng.* , Tokyo Inst. Technol.

Sornette D. (2000) : *Critical Phenomena in Natural Sciences.* 434 p., Springer.

Tomioka N. and Okuchi T. (2017): A new high-pressure form of Mg2SiO4 highlighting diffusionless phase transitions of olivine. *Scientific Reports*, 7, No. 17351.

Torpey M.E. (2016): Investigation of the Maule, Chile rupture zone using seismic attenuation tomography and shear wave splitting methods. *Dissertation Univ. Florida*, 151 p. http://ufdc.ufl.edu/UFE0049910/00001

Uta P. (2017): Recent Intraplate Earthquakes in Northwest Germany - Glacial Isostatic Adjustment and/or a Consequence of Hydrocarbon Production? *Dissertation Univ. Hannover*, 199 p. https://doi.org/10.15488/9088